THE JOURNAL OF PHYSICAL CHEMISTRY C

Article

pubs.acs.org/JPCC

Finding Correlations of the Oxygen Reduction Reaction Activity of Transition Metal Catalysts with Parameters Obtained from Quantum Mechanics

Ted H. Yu,[†,‡] Timo Hofmann,[§,∥] Yao Sha,[†] Boris V. Merinov,*[,†] Deborah J. Myers,[⊥] Clemens Heske,[§,#,○,△] and William A. Goddard, III*[,†]

[†]Materials and Process Simulation Center, m/c 139-74, California Institute of Technology, 1200 East California Blvd., Pasadena, California 91125, United States

[‡]Department of Chemical Engineering, California State University, 1250 Bellflower Blvd., Long Beach, California 90840, United States

[§]Department of Chemistry, University of Nevada Las Vegas, 4505 South Maryland Parkway, Las Vegas, Nevada 89154-4003, United States

[∥]Bundeswehr Research Institute for Materials, Fuels, and Lubricants, Institutsweg 1, 85435 Erding, Germany

[⊥]Chemical Sciences and Engineering Division, Argonne National Laboratory, 9700 South Cass Avenue, Argonne, Illinois, 60439, United States

[#]Institute for Photon Science and Synchrotron Radiation (IPS), Karlsruhe Institute of Technology, Hermann-v.-Helmholtz-Platz 1, 76344 Eggenstein-Leopoldshafen, Germany

[○]ANKA Synchrotron Radiation Facility, Karlsruhe Institute of Technology, Hermann-v.-Helmholtz-Platz 1, 76344 Eggenstein-Leopoldshafen, Germany

[△]Institute for Chemical Technology and Polymer Chemistry, Karlsruhe Institute of Technology, Engesserstr. 18/20, 76128 Karlsruhe, Germany

Supporting Information

ABSTRACT: To facilitate a less empirical approach to developing improved catalysts, it is important to correlate catalytic performance to surrogate properties that can be measured or predicted accurately and quickly, allowing experimental synthesis and testing of catalysts to focus on the most promising cases. Particularly hopeful is correlating catalysis performance to the electronic density of states (DOS). Indeed, there has been success in using just the center of the d-electron density, which in some cases correlates linearly with oxygen atom chemisorption energy, leading to a volcano plot for catalytic performance versus "d-band center". To test such concepts we calculated the barriers and binding energies for the various reactions and intermediates involved in the oxygen reduction reaction (ORR) for all 12 transition metals in groups 8−11 (Fe−Cu columns). Our results show that the oxygen binding energy can serve as a useful parameter in describing the catalytic activity for pure metals, but it does not necessarily correlate with the d-band center. In addition, we find that the d-band center depends substantially on the calculation method or the experimental setup, making it a much less reliable indicator for ORR activity than the oxygen binding energy. We further examine several surfaces of the same pure metals to evaluate how the d-band center and oxygen binding energy depend on the surface.

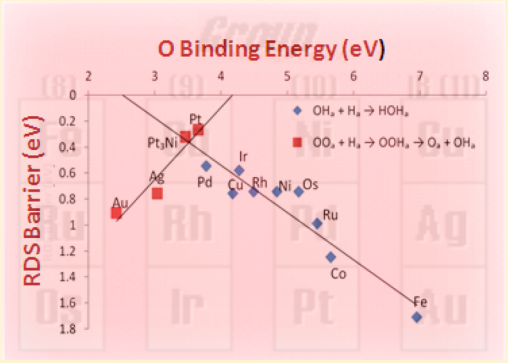

1. INTRODUCTION

For the purpose of guiding the discovery of new catalysts, it is useful to develop simple concepts and measures that can suggest compositions most likely to improve performance. Particularly promising in this regard is the electronic density of states (DOS) that can be measured using photoelectron spectroscopy[1,2] (PES) and calculated from quantum mechanics (QM) using density functional theory (DFT). Thus, the DOS could be a promising screen for potential new catalysts that may offer better performance than current catalysts.[3,4]

A particularly important application is to polymer electrolyte membrane fuel cells (PEMFCs). For even the most successful catalyst, expensive Pt, the oxygen reduction reaction (ORR) is

Received: July 18, 2013
Revised: November 21, 2013
Published: November 25, 2013

ACS Publications © 2013 American Chemical Society

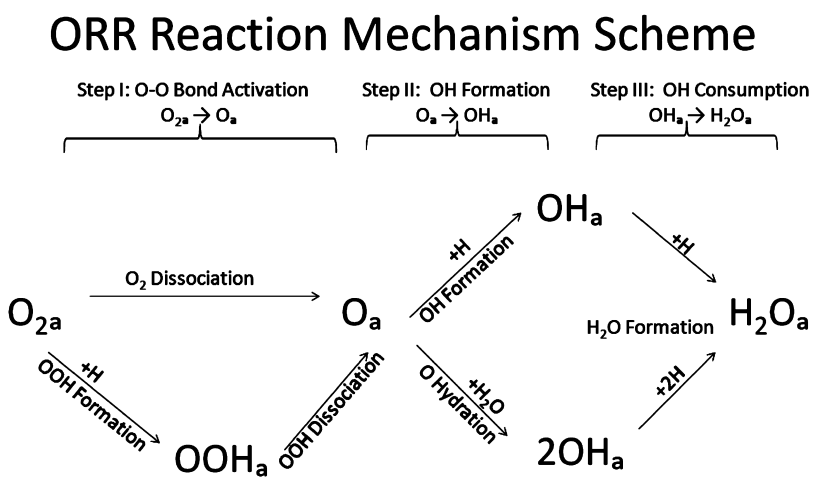

Figure 1. Scheme of the ORR mechanism: O_{2a} dissociates to form atomic O_a or associates with H_a to form OOH_a followed by dissociation to form O_a and OH_a. Atomic O_a reacts with either H_a or H_2O_a to form OH_a, and OH_a reacts with H_a to form H_2O_a.

over 2 orders of magnitude slower than the anode reaction, requiring so much catalyst that these fuel cells are not economical.[5] To make PEMFCs commercially viable, new ORR catalysts, such as alloys of earth abundant metals, with similar or improved performance compared to Pt are needed.

d-Band centers derived from both theory and experiment have been used to correlate trends in the binding energy of oxygen species and fuel cell activity.[6−11] The d-band center is defined as $E_d - E_F$,[4] where E_d is the energy of the average occupied d-electron density and E_F is the Fermi energy. In cases where the catalysts are similar, the plot of the d-band center of various alloys versus their activity has yielded a volcano plot with the optimal d-band center at the top of the volcano, corresponding to the highest activity.[6,7,11] One of the key contributions of the d-band center theory is that it provides an explanation of how a subsurface atom can affect the binding energy. Even though the subsurface atom does not bind directly to the adsorbate, it can change the d-band center at the surface atom. This change in the d-band center at the surface atom, in turn, may change how the surface atom interacts with the adsorbate. Thus, the subsurface atom, which is a "spectator", might subtly change the binding energy of the catalyst. This d-band theory was successfully used to rationalize why PEMFC alloy catalysts, such as Pt_3Ni or Pt_3Co,[12,13] that have 100% Pt on the surface layer (so-called Pt-skin), improve ORR catalytic activity over that of pure Pt.

This success has led to additional fuel cell research applying the d-band center theory as a tool to propose replacement of Pt with less expensive and more efficient ORR catalysts, such as Pt-based alloys,[6,7,11,14,15] cheaper non-Pt alloy catalysts,[16−18] Pt monolayer core−shell catalysts,[8,19,20] or Pt sandwich catalysts.[9,21] Since the d-band center theory had some success in rationalizing compositions with improved catalytic activity, for similar materials, several attempts have been undertaken to generalize this theory and apply it also to dissimilar catalysts.[20,22,23]

Recently we reported[24] the bulk density of states (DOS) for eight transition metal catalysts both from DFT theory and experimental photoelectron spectroscopy (PES). For each metal, the shapes of the experimental valence band structure and theoretical DOS have similar features. However, we found that the bulk d-band center from the standard flavor of DFT (PBE) did not match experiment. In a comment on our paper, Norskov and co-workers[25] stressed that the d-band center theory should not be applied to correlate catalytic activity with d-band centers for a broad variety of metals, rather it should only be used when the matrix element is constant[20] or approximately constant. This is because the theoretical coupling matrix between different pure metals varies too greatly for d-band center theory to apply. Since d-band center theory works only if there is a coupling matrix as a common baseline, one should use it only to examine small variations in the catalyst composition. In this case, the changes in the d-band center might correlate with the changes in binding energy.

Despite this comment clearly stating that the d-band center model is not expected to predict relative activity between different pure metals, several papers (see, for instance, ref 22) have compared d-band centers between different pure metals and report a linear correlation of the O chemisorption energy with the d-band center for Fe, Co, Ni, and Cu (including metals with different crystal structures and electronic character). Other authors have also attempted to establish a universal relationship between the d-band center and binding energy with applications to very different catalysts.[14,20,23] They assumed the existence of a good correlation between the d-band center and catalyst activity without first establishing the correlation between the d-band center and O chemisorption energy.[23,26] Even in the case where the catalysts have similar compositions, the d-band center is a very approximate measure of the chemisorption energy of the critical intermediate, say O. Actually, the chemisorption energy is as easily evaluated as the d-band center and much more relevant for catalyst activity. As shown in our previous publication[27] and in the comment to it,[25] the universal correlation between the d-band center and catalytic activity does not exist. In this paper, we report calculations of the various reaction intermediates involved in ORR for twelve pure metals of columns 8−11 and compare the various chemisorption energies with the d-band center and other measures of the DOS.

In order to understand how the O chemisorption energy relates to the ORR activity for these various metals, we consider the reaction barrier for the rate-determining step (RDS)[16,28,29] as a measure of the catalyst activity, assuming that the highest energy barrier determines the RDS and hence the reaction rate. Here we assume that the relative rates correlate inversely with the highest barrier. For the various metals studied, we examine

dx.doi.org/10.1021/jp4071554 | J. Phys. Chem. C 2013, 117, 26598−26607

Table 1. Calculated NEB Barriers (eV) of the ORR Surface Reactions[a]

barrier	metal											
	Fe	Co	Ni	Cu	Ru	Rh	Pd	Ag	Os	Ir	Pt	Au
O_2 dissociation: $O_{2a} \rightarrow 2O_a$	0.00	0.00	0.10	0.15	0.03	0.14	0.77	0.93	0.02	0.00	0.58	2.11
OOH formation: $O_2 + H_a \rightarrow OOH_a$	n/a[b]	0.51	0.58	0.36	0.70	0.48	0.49	0.22	0.67	0.56	**0.28**	0.00
OOH dissociation: $OOH_a \rightarrow O_a + OH_a$	n/a[b]	0.05	0.00	0.54	0.00	0.00	0.29	**0.76**	0.00	0.62	0.14	**0.91**
OH formation: $O_a + H_a \rightarrow OH_a$	0.00	0.40	0.44	0.00	1.06	0.60	0.19	0.00	1.62	0.84	0.72	0.16
O hydration: $O_a + H_2O_a \rightarrow 2OH_a$	0.00	0.57	0.51	0.37	0.24	0.39	0.44	0.67	0.17	0.27	0.27	0.27
H_2O formation: $OH_a + H_a \rightarrow H_2O_a$	**1.71**	**1.25**	**0.75**	**0.76**	**0.99**	**0.74**	**0.54**	0.60	0.75	0.58	0.11	0.31
RDS	1.71	1.25	0.75	0.76	0.99	0.74	0.54	0.76	0.75	0.58	0.28	0.91

[a]According to our mechanism, some of these reactions can be circumvented. The rate determining step (bold numbers) for each metal is the largest barrier of the relevant reactions, which is our measure of the ORR rate. [b]OO_a and OOH_a are not stable adsorbates on Fe (110).

Table 2. Binding Energies (BE, eV) of the ORR Intermediates

BE	metal											
	Fe	Co	Ni	Cu	Ru	Rh	Pd	Ag	Os	Ir	Pt	Au
H	2.78	2.80	2.46	2.42	2.83	2.67	2.70	1.99	2.70	2.76	2.67	1.87
HOH	0.78	0.18	0.35	0.19	0.45	0.33	0.25	0.13	0.43	0.32	0.22	0.12
O	6.96	5.67	4.85	4.18	5.45	4.49	3.78	3.04	5.17	4.28	3.68	2.42
OH	5.22	3.61	3.18	2.85	3.37	2.92	2.53	2.35	3.13	2.74	2.28	1.81
OO	n/a[a]	1.87	1.40	0.56	1.94	1.37	0.78	0.06	1.79	1.28	0.46	0.17
OOH_a	n/a[a]	1.88	1.74	1.11	1.92	1.52	1.15	0.57	1.71	1.52	1.06	0.25

[a]OO_a and OOH_a are not stable adsorbates on Fe (110).

the intermediates in the ORR: $O_{2a} \rightarrow O_a \rightarrow OH_a \rightarrow H_2O_a$,[28−32] as outlined in Figure 1. A previous study[30] that compared theoretical rates versus O binding energy of transition metals used a microkinetic model that includes physical assumptions to model the ORR activity. For example, rotational constants based on 3-D rotation of an O_2 gas molecule were used to model the dissociation of O_2 on a catalyst surface, where the 3-D rotation of the O_2 molecule would be restricted. Our model, described in detail in the following sections, differs from the previously published model because the estimated rates are obtained from DFT calculations that simulate directly the bond formation and dissociation.

We find that the d-band center varies substantially depending on the calculation method or the experimental setup, making it a less reliable indicator for the ORR activity than the oxygen binding energy. We further examine ORR for several surfaces of some pure metals to evaluate whether the d-band center can predict the dependence of binding energy on a surface orientation.

2. COMPUTATIONAL METHODS

Periodic QM calculations were carried out using the SeqQuest code,[33,34] which employs Gaussian basis functions at the optimized double-ζ plus polarization level (rather than the plane-wave basis often used in periodic systems). We use DFT with the Perdew−Burke−Ernzerhof (PBE)[35] approximation of the generalized gradient approximation (GGA)[36] exchange-correlation functional. The up-spin orbitals are allowed to be optimized independently of the down-spin orbitals (spin-unrestricted DFT). The small core pseudopotentials with angular momentum projections[37,38] are applied in our calculations.

The d-band and total band structures were analyzed using the SeqQuest post analysis code,[34] which determined the center of the d-band. The bands are further broadened by convolution with a 0.5 eV FWHM Gaussian function to approximate the experimental Gaussian broadening and Lorentzian lifetime broadening. We use the NEB[39] function of SeqQuest to calculate reaction barriers of the intermediate reactions. The NEB approach starts with the minimized structure for the reactant and for the product for a particular postulated pathway and then minimizes the energy for 5−7 proportional steps between the reactant and product, producing a minimum energy pathway between them.

The bulk and surface crystal structures for each metal correspond to the lowest-energy structures and the corresponding lowest-energy surface. The bulk structures are bulk-centered cubic (BCC) for Fe, hexagonal close-packed (HCP) for Co, Ru, and Os, and face-centered cubic (FCC) for Ni, Cu, Rh, Pd, Ag, Ir, Pt, and Au.[40] The surface orientations are (110) (Fe), (0001) (Co, Ru, Os), and (111) (Ni, Cu, Rh, Pd, Ag, Ir, Pt, Au).[40] All surfaces are modeled two-dimensionally infinite periodic slab with four atoms per cell (25% coverage) and six layers of atoms with the bottom layer fixed. Because of the Gaussian basis functions, a vacuum layer is not necessary for two-dimensional calculations. The real space grid density is 5 points per angstrom, while the reciprocal space grid is $5 \times 5 \times 0$ for slab calculations. The bulk reciprocal space grid is $10 \times 10 \times 10$.

3. RESULTS AND DISCUSSION

3.1. ORR Activity versus Binding Energy. To estimate the ORR activity of different metals, we outline our mechanistic model from QM energetic barriers.[16,28,29] It is important to examine the bond formation and breaking mechanisms for ORR. Based on the ORR scheme presented in Figure 1, we examine the individual barriers of six reactions possibly relevant for ORR:

(1) O_2 dissociation: $O_{2a} \rightarrow 2O_a$
(2) OOH formation: $O_{2a} + H_a \rightarrow OOH_a$
(3) OOH dissociation: $OOH_a \rightarrow O_a + OH_a$
(4) OH formation: $O_a + H_a \rightarrow OH_a$

dx.doi.org/10.1021/jp4071554 | J. Phys. Chem. C 2013, 117, 26598−26607

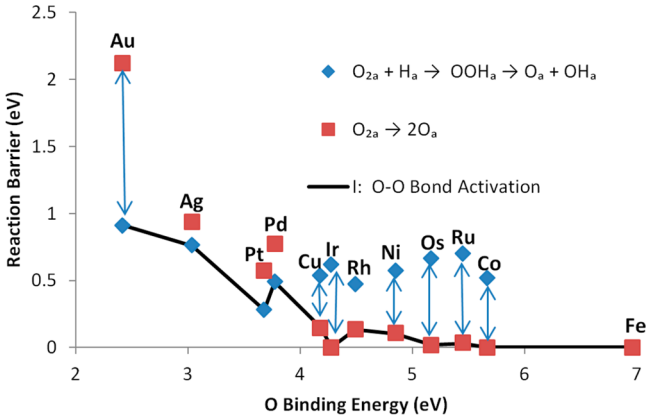

Figure 2. Catalyst-specific barriers of process I (O−O bond activation) of ORR: OOH formation + dissociation ($OO_a + H_a \rightarrow OOH_a \rightarrow O_a + OH_a$, blue diamonds) and O_2 dissociation ($O_{2a} \rightarrow 2O_a$, red squares) as a function of atomic O binding energy. A line runs through the lower of the two barriers. The difficulty of O−O bond activation decreases as O binding energy increases.

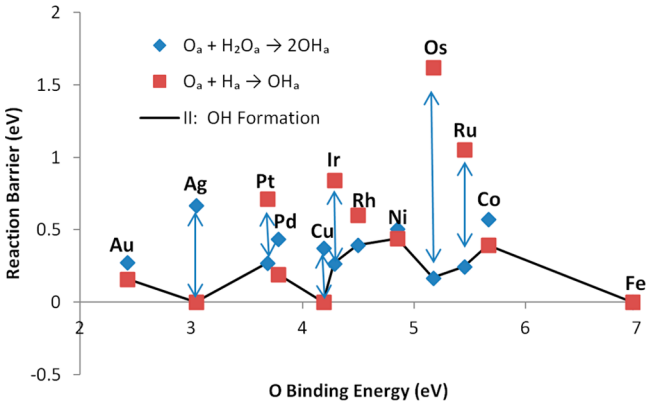

Figure 3. Catalyst-specific barriers of process II (OH formation) of ORR: OH formation ($O_a + H_a \rightarrow OH_a$, red squares) and O hydration ($O_a + H_2O_a \rightarrow 2OH_a$, blue diamonds) as a function of atomic O binding energy. A line runs through the lower of the two barriers. The reaction barriers are not observed to be correlated with the O binding energy.

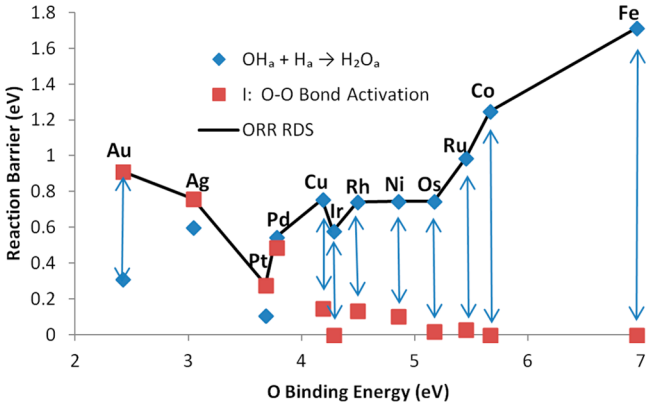

Figure 4. Catalyst-specific barriers of process III (OH consumption) of ORR: H_2O formation ($OH_a + H_a \rightarrow O_a + H_2O_a$, blue diamonds). The difficulty of H_2O formation increases as O binding energy increases. O−O bond activation is plotted in comparison. A line runs through the higher of these two barriers. This line represents the ORR RDS barrier for each pure metal catalyst.

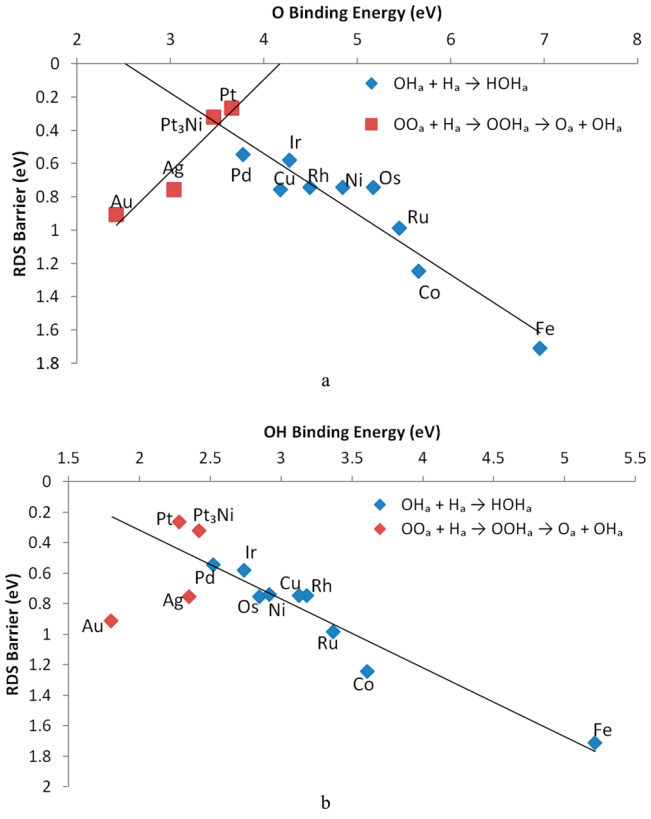

Figure 5. Plot of the atomic O (a) and OH (b) binding energy with the RDS barrier of ORR from our mechanism. As the binding energies decrease, the barriers for $OO_a + H_a \rightarrow OOH_a + OH_a$ increase. As the binding energies increase, the barriers of $OH_a + H_a \rightarrow HOH_a$ increase. There is a linear trend when plotting the H_2O formation RDS barrier versus OH and O binding. A similar linear trend is observed when plotting the RDS barrier of $OO_a + H_a \rightarrow OOH_a + OH_a$ versus O binding, but this is not observed versus OH binding.

(5) O hydration:[28] $O_a + H_2O_a \rightarrow 2OH_a$
(6) H_2O formation: $OH_a + H_a \rightarrow H_2O_a$

The transition state for each step was located by starting with the lowest energy configuration of the reactant and exploring all plausible pathways toward the reaction product. The path with the lowest barrier determines the transition state.

Table 1 compares the calculated barriers for these 6 reactions for each of the 12 metals. The RDS is taken as the highest predicted barrier in the mechanism for each metal, with the most energetically favorable geometry as the starting point.[40] For all of the metals, other than Pt, Au, and Ag, the RDS is H_2O formation. Indeed, Table 1 predicts Pt to have the fastest rate with the lowest ORR RDS of 0.28 eV (OOH formation). The next best is Pd with a RDS of 0.54 eV (H_2O formation). Table 2 lists the binding energies for various intermediates[40] of the different metals. The most electronegative elements Pt, Au, and Ag have the weakest O and OH binding energy for the corresponding metals.

Next, we develop some rationale to better understand the differences in reaction barriers for the metals and why it relates to the binding energy. We can expect that the binding energy of O and OH are strongly correlated[30] because both involve electron transfer to the O p orbital. This correlation between O and OH binding has a profound effect on trends in three chemical processes of the ORR reaction which are:

dx.doi.org/10.1021/jp4071554 | J. Phys. Chem. C 2013, 117, 26598−26607

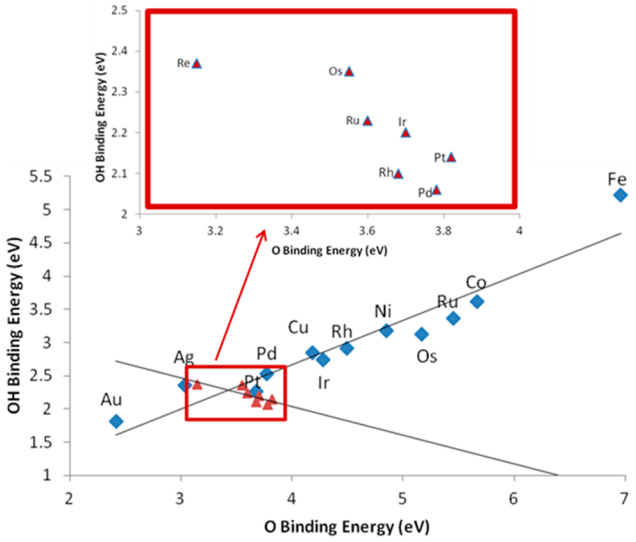

Figure 6. Plot of O and OH binding energies for pure metals from this work (blue diamonds and element labels) and Pt sandwich catalysts from Xin et al.[41] (red triangles), both as an overview (top graph) and on an expanded O binding energy scale (red rectangle and bottom graph). The element label next to the red triangle represents the noble metal substrate for the Pt sandwich catalyst. When sandwich catalysts and pure metals are compared, the O and OH binding energies have opposite correlation trends.

I. $O_{2a} \rightarrow O_a$: O−O bond activation, which can occur via two mechanisms: O_2 dissociation and OOH formation followed by OOH dissociation.
II. $O_a \rightarrow OH_a$: OH formation proceeds via two mechanisms as well: OH formation and O hydration.
III. $OH_a \rightarrow H_2O_a$: OH consumption has only one mechanism, H_2O formation, for this process.

3.1.1. Process I. Process I in the ORR reaction involves activating the O−O bond by O_2 dissociation ($O_{2a} \rightarrow 2O_a$) or by OOH formation + dissociation ($O_{2a} + H_a \rightarrow OOH_a \rightarrow O_a + OH_a$). In either case, process I becomes more exothermic as increasing O binding energy. Figure 2 compares these two possible pathways for the O−O bond activation. From Figure 2, we see that $O_{2a} + H_a \rightarrow OOH_a \rightarrow O_a + OH_a$ is favored for catalysts with weak O binding (Au, Ag, Pt, Pd), while $O_{2a} \rightarrow 2O_a$ is favored for the remaining catalysts with strong O binding. The observed trend is related to the formation of the OOH_a intermediate which becomes less favorable as the O binding energy increases, and for the highest O binding catalyst, Fe, OOH_a is completely unstable.

3.1.2. Process II. Figure 3 plots the barriers for the second process of ORR, OH formation. We find that this process weakly depends on the binding energy of O. The reason for this is that for pure metals the binding energy of the reactant, O, and product, OH, are directly correlated. There are two possible reactions for the OH formation: OH addition, $O_a + H_a \rightarrow OH_a$, and O hydrolysis, $H_2O_a + O_a \rightarrow 2OH_a$[28] (see Figure 3). We assume that the energetically lower pathway is favored. In Figure 3 it is indicated by the black solid line, which does not exceed 0.5 eV for the cases studied. OH formation becomes an important RDS for Pt sandwich catalysts, where the binding energy of O and OH are not correlated.[41] The barriers calculated indicate the difficulty of forming OH_a, whether or not the source of the H and H_2O originate on the surface or in the solution. The inclusion of the O hydrolysis reaction[28] is critical to our overall analysis. Including this reaction for Pt lowers the barrier of Process II from 0.72 to 0.27 eV.

3.1.3. Process III. The third ORR process is OH consumption. We plot the barrier for this reaction in Figure 4. This barrier becomes less favorable with increasing OH binding energy and hence it correlates with O binding due to the correlation between the binding energy of O and OH. Since OH_a is the reactant, the barrier for this reaction increases as the O and OH binding energy increases.

We also plot in Figure 4 the barrier for the first ORR process, O−O bond activation. The second ORR process to form OH_a (Figure 3) was found to be non-rate-limiting, because in all cases either I or III in the ORR mechanism has the highest barrier.

3.1.4. ORR Rate-Determining Step (RDS). Figure 5 shows the ORR RDS barrier versus the O and OH binding energies. Two solid lines in Figure 5 correspond to the linear fit for each RDS barrier as a function of binding energy. A volcano-shaped trend with Pt near the top might be identified. The plot shows that the RDS is the first ORR process at O binding energies lower than that of Pt. When the O binding energy is higher than that of Pt, the RDS is the third ORR process, OH consumption. In this way, we are able to estimate the overall ORR rate proceeding from the binding energy of O. The linear fit is not good when plotting the binding energy of OH versus the RDS for Au, Ag, Pt_3Ni, and Pt. This is because the O−O activation depends more on the O binding energy. It was previously shown that Ag has weaker O binding and stronger OH binding when compared to Pt and does not have good linear O and OH binding energy correlation.[30]

There are various works that performed comprehensive ORR reaction barrier studies of different transition metals. For example, Ford et. al[42] investigated various ORR reactions on different transition metals and found linear correlation between the barrier and the O binding energy. The result of this study differs, in that the results demonstrate a volcano plot with Pt clearly as the best catalyst when comparing the RDS (the O hydration step with a barrier of 0.28 eV) with other catalysts (for comparison, Pd RDS = 0.54 eV). This shows the importance of including the O hydration reaction[28] ($O_a + H_2O_a \rightarrow 2OH_a$), which is an alternative to direct OH formation ($O_a + OH_a \rightarrow 2OH_a$). Without including the O hydration reaction, the RDS for Pt would be higher (0.72 eV), than that for Pd.

While the results show good agreement when comparing pure metals, this analysis should not be applied to particular catalysts for which O and OH binding energies are not correlated. This can occur for nonpure metals. For example, Zhang et al.[8] observed linear trends for the DFT-calculated O_2 dissociation and OH formation barriers versus atomic O binding energy for a group of catalysts consisting of Pt monolayers (ML) on different metal substrates: Pt_{ML}/Ru-(0001), Pt_{ML}/Ir(111), Pt_{ML}/Rh(111), Pt_{ML}/Au(111), and Pt_{ML}/Pd(111). However, for the pure metals studied herein, the OH formation barrier does not continuously increase with oxygen binding (Figure 3). This difference in the catalytic trend between Pt monolayer catalysts on substrates from pure metals exists because the O and OH binding energies do not exhibit a linear correlation.[40] It even exhibits a reverse correlation[41] in the case of Pt sandwich catalysts. In contrast, for pure metal catalysts, the binding energies of O and OH are directly correlated.[30] The trends in binding energy of O and OH for the pure metals and Pt sandwich catalysts are plotted in Figure 6.

dx.doi.org/10.1021/jp4071554 | J. Phys. Chem. C 2013, 117, 26598−26607

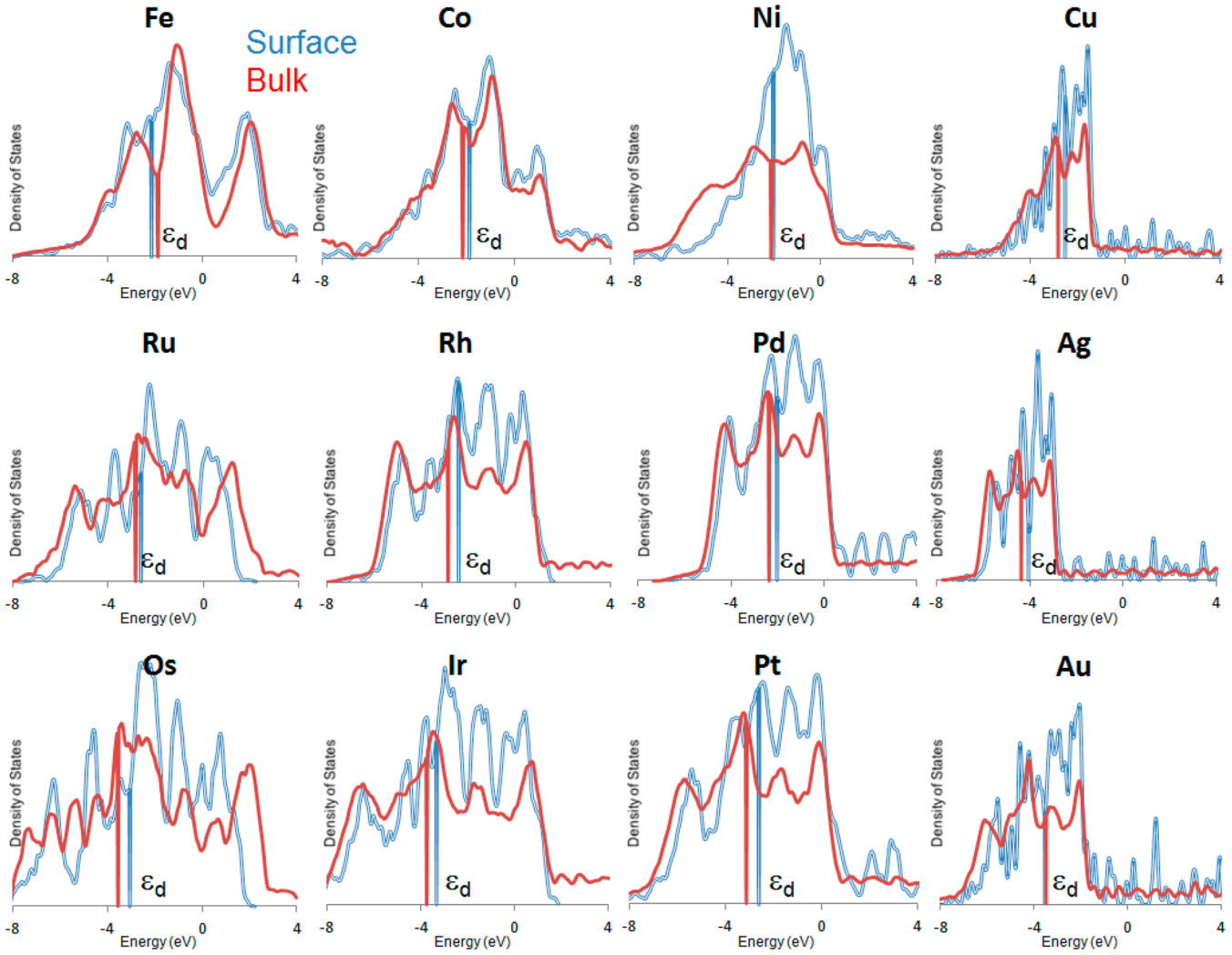

Figure 7. Comparison of the calculated bulk and surface total DOS of twelve pure metals. The density of state (e^-/energy) is plotted vs the energy (Fermi energy at 0). The bulk bands (red) show the total DOS for the metal with its bulk crystal structure (BCC, Fe; HCP, Co, Ru, Os; FCC, Ni, Cu, Rh, Pd, Ag, Ir, Pt, Au). The surface bands show the total DOS (blue) for the top layer of the most favorable surface orientation: (110), Fe; (001), Co, Ru, Os; (111), Ni, Cu, Rh, Pd, Ag, Ir, Pt, Au. The vertical line corresponds to the position of the bulk and surface d-band centers.

Table 3. Comparison of the Band Centers (in eV) Derived from DOS with Those in Literature[a]

	current work				reference d-band center	
	surface		bulk			
element	total	d-band	total	d-band	theory	experiment
Fe	−2.34	−2.16	−2.14	−1.88	−0.92[3]	−1.55[24]
Co	−2.10	−1.89	−2.54	−2.16	−1.17,[3] −2.0[43]	−1.54[24]
Ni	−2.24	−2.03	−2.35	−2.09	−1.29,[3] −1.48,[4] −1.7[43]	−1.20[24]
Cu	−2.64	−2.51	−3.02	−2.83	−2.4,[43] −2.67[3,4]	−3.05[24]
Ru	−2.69	−2.63	−3.04	−2.85	−1.41,[3] −2.7[43]	
Rh	−2.54	−2.45	−3.00	−2.86	−1.73,[3] −2.3[43]	
Pd	−2.13	−2.03	−2.44	−2.30	−1.8,[43] −1.83[3]	−2.09[24]
Ag	−3.97	−4.07	−4.31	−4.37	−4.0,[43] −4.30[3]	−5.28[24]
Os	−3.21	−3.07	−3.89	−3.55		
Ir	−3.11	−3.29	−4.00	−3.75	−2.11,[3] −2.9[43]	
Pt	−2.79	−2.60	−3.38	−3.13	−2.25,[3] −2.4,[43] −2.75[4]	−2.54,[10] −2.94,[24] −4.77,[45] −2.75[14]
Au	−3.53	−3.47	−4.06	−3.94	−3.5,[43] −3.56,[3] −3.91[4]	−4.45[24]

[a]The "total" column contains all s, p, and d electronic contributions, while the "d" column contains just the d states (d-e_g and d-t_{2g}). The "Bulk" column gives the results of three-dimensional crystal calculations. The "Surface" column represents the topmost layer of the most favorable surface and is derived from slab calculations. The "Theory" reference d-band centers are surface d-bands. The experimental reference d-band centers contain contributions from both bulk and surface.

dx.doi.org/10.1021/jp4071554 | J. Phys. Chem. C 2013, 117, 26598−26607

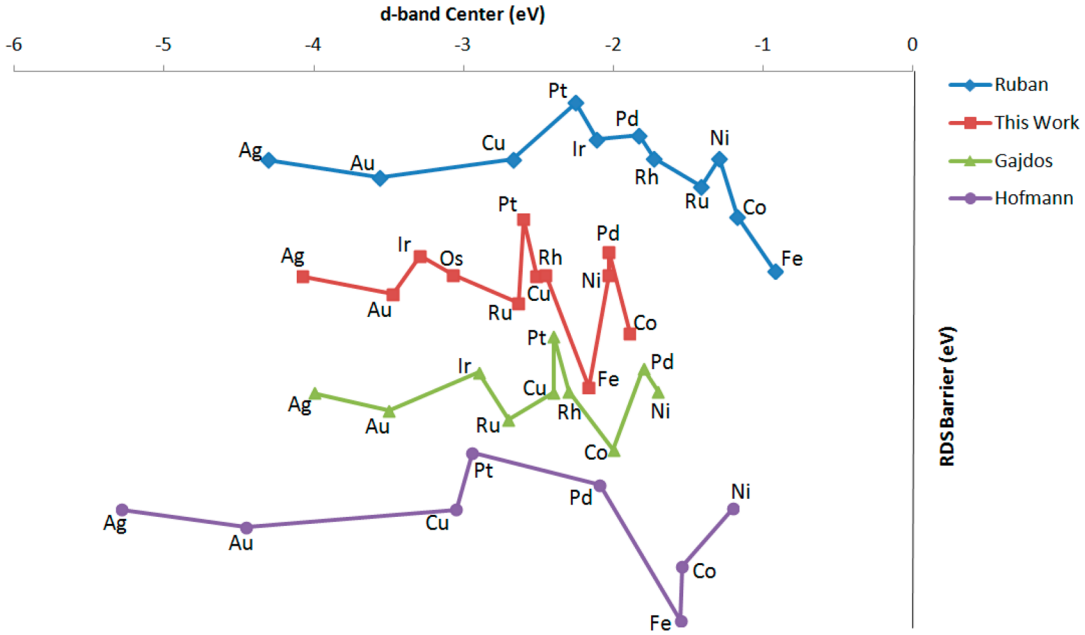

Figure 8. Plot of the ORR critical barrier (with offset) vs the theoretical and experimental d-band center for different pure metal catalysts. Theoretical d-band centers of Ruban et al.[3] resemble an "N"-shaped plot. The plots for the theoretical d-band centers of Gajdos et al.[43] and this work are best described as scattered zigzags. Experimental d-band centers of Hofmann et al.[27] look somewhat like a "W"-shaped plot. Large differences exist for the d-band centers of pure metals when different methods are used to determine it.

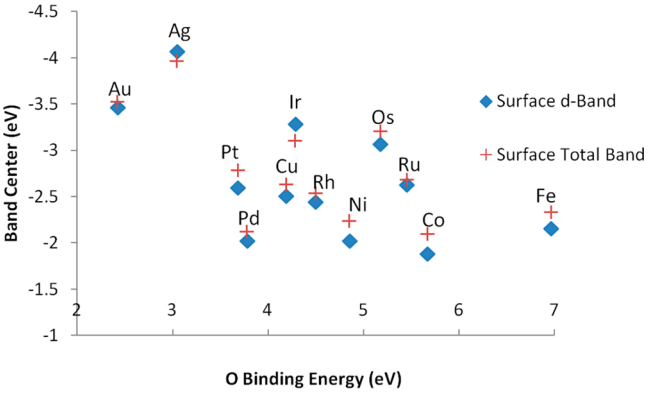

Figure 9. Trending the O binding energy of twelve metals vs their surface band centers. The lack of linearity between the binding energy and band centers indicates why plotting the d-band center vs ORR activity does not exhibit a volcano shape.

3.2. Density of State and d-Band Center. The total DOS from DFT calculations on both the bulk system and the surface monolayer are shown for 12 metals in Figure 7. In Table 3, their band centers are compared to those found in literature.[3,4,10,24,43] The band centers are calculated for both the three-dimensional bulk and two-dimensional slab DOS ("surface DOS"), as outlined previously.[3,4]

From Figure 7, we see that the bulk DOS differs from the surface DOS. This is ascribed to the larger atom coordination for the bulk atoms versus surface atoms, which arises because the under-coordination of the surface atoms leads to a narrower band.[44] The d-band center of the bulk and surface is shown as a vertical line in Figure 7 and can vary by as much as 0.5 eV, as in the Pt case. The bulk DOS is very relevant when comparing with experiment because the "true" experimental electronic structure at a surface is a combination of both the electronic bulk states, as well as those contributed by the outermost surface atoms.[27]

Our computed surface d-band centers (Table 3) are in good agreement with those reported by Gajdos et al.[43] (average absolute difference of 0.17 eV), which is expected because we use the same DFT functional, PBE[35] (although we used the Gaussian basis set of SeqQuest, while Gajdos et al. used the plane-wave basis set of VASP). In contrast, our result disagrees significantly with that of Ruban et al.[3] (average absolute difference of 0.62 eV), who used the linear muffin-tin orbital method within the atomic sphere approximation (LMTO-ASA), which is far less accurate. Unfortunately, since the d-band centers of pure metals published by Ruban et al.[3] were the first thorough theoretical determination of d-band centers, these values are the ones usually cited by experimentalists.[20,23]

Comparing the experimental d-band centers with the various theoretical results, the average absolute difference is 0.59 eV versus Ruban et al.,[3] 0.68 eV versus Gajdos et al.,[43] 0.62 eV comparing to our surface d-band centers, and 0.49 eV comparing to our bulk d-band centers. This large difference between experimental and theoretical d-band centers for pure metals makes these quantities less useful for predicting reactivity and requires performing an offset correction to adjust the theoretical DOS to the experimental ones.

3.3. d-Band Centers for Different Pure Metals. Figure 8 compares our measure of the ORR activity based on the RDS barriers vs the experimental and calculated d-band centers from Table 3.[3,24,43] Indeed, comparing the plots in Figure 8, only the d-band centers derived from ref 3 give some resemblance of a volcano plot. The major outlier for all cases is Ag, which shows better activity than Au, but has the d-band center much farther away from that of Pt. This, in turn, makes the plot of the d-band centers derived from ref 3 look like an "N".

The ORR activity versus the d-band center from our work and that of Gajdos et al.[43] leads to what is best described as a zigzag plot. The experimental d-band center plot from our

dx.doi.org/10.1021/jp4071554 | J. Phys. Chem. C 2013, 117, 26598−26607

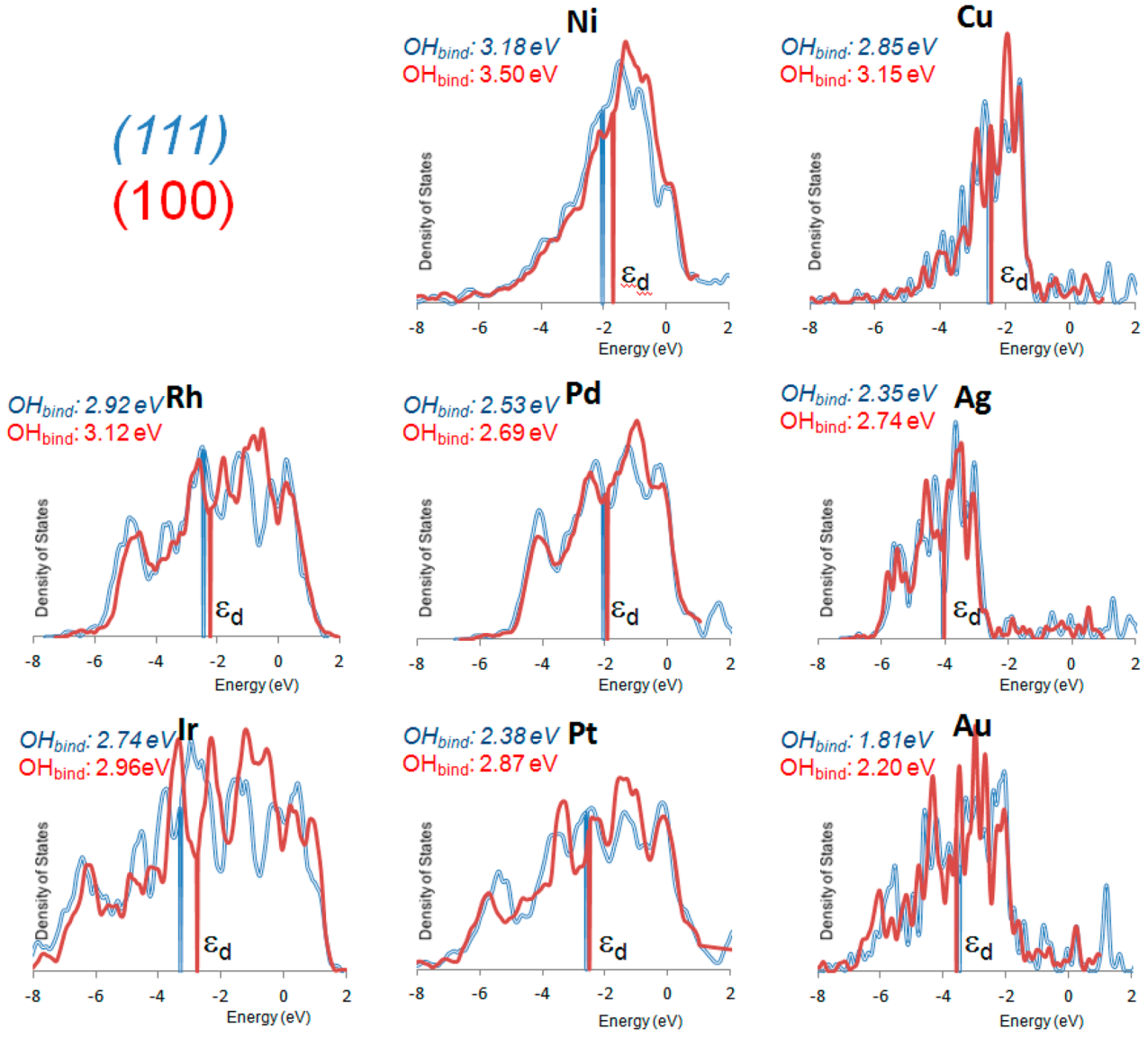

Figure 10. Comparison of the (111) and (100) topmost surface DOS for different pure metals. The corresponding OH binding energies are given in the upper left of each graph with the (111) orientation italicized. The vertical line represents the position of the corresponding (100) or (111) surface d-band center. The Fermi energy is set to zero. The OH binding energy of the (100) surface is stronger than that of the (111) surface in all cases. The d-band centers of Pt, Au, and Ag are very similar even though the binding energy changes dramatically between the (100) and (111) surface orientations.

recently published work[27] somewhat resembles a "W". Therefore, large variances are observed in the results on the d-band centers, and none of the plots suggests that there is good correlation between the d-band center and ORR activity when comparing pure metals.

From the results of Figure 8, it is important to further analyze why the d-band center model breaks down for pure metal catalysts. We divided the question about how the d-band center correlates to the ORR activity into two pieces: (1) correlation between d-band center and binding energy, (2) correlation between binding energy and ORR activity. Figure 5 demonstrates that the second correlation between binding energy and activity is valid for transition metals.

In Figure 9, we plot the atomic O binding energy versus the surface d-band center for the 12 metals. Clearly, there is no correlation between them. Figure 9 demonstrates that the breakdown in the correlation between the d-band center and ORR activity is likely due to the poor correlation between the d-band center and binding energy when comparing transition metals. Previous studies on d-band centers that reported better linear correlations with binding energy compared either similar catalysts or a small set of pure metals.[22] For example, Adzic et al.[8] and Menning at al.[9] used DFT-GGA methods to determine d-band centers and found a good linear fit with oxygen binding energy. In ref 8, the d-band centers of different Pt monolayer catalysts were compared with different metals in the sublayer (Ru, Ir, Rh, Au, Pt, Pd). In ref 9, the catalysts have Pt sandwich structures, in which the center of the sandwich consists of 3d metals along the same row of the periodic table (Ti, V, Cr, Mn, Fe, Co, and Ni).

From a practical viewpoint, the calculated O binding energy might be a better parameter than the calculated d-band center, to estimate the ORR activity, because as we showed above, the O binding energy better correlates with the ORR activity quantitatively.

dx.doi.org/10.1021/jp4071554 | J. Phys. Chem. C 2013, 117, 26598−26607

3.4. d-Band Centers for Different Surface Orientations. Next, we consider the case of different surface orientations for the same catalyst, comparing binding energy versus d-band center. Earlier, the d-band center model has already been used to explain the difference in the activity of the same catalyst for different orientations.[14] In Figure 10, the DOS for the (111) and (100) surfaces are plotted for eight FCC metals. Comparing the OH binding energies,[40] we see that they vary for different orientations, but the binding energy for the (100) surface is always higher than that for the (111) surface. According to the d-band center model, the weaker-bonding (111) orientation should have a higher d-band center ($\varepsilon_d - \varepsilon_F$), while the (100) DOS should have a lower d-band center. For the case of Pt, Ag, and Au, the binding energy between the (111) and (100) surfaces varies by ~0.4 eV, but the d-band center positions are about the same (Figure 10). We also found the RDS barrier for the Pt (100) surface to be much higher (0.52 eV) than the RDS barrier (0.28 eV) for the Pt (111),[40] which means identical d-band center values have different predicted activity. Thus, the quantitative correlation between the binding energy and d-band center for different orientations is not observed.

4. CONCLUSION

Using a detailed description of the ORR mechanism, we establish the relationship between the binding energy and ORR activity for a number of pure metals. We compare this relationship with the d-band center theory, confirming that it is valid only when the d-band center has good correlation with binding energy and varies with it linearly. Testing the linearity of the binding and d-band center, we find at least two cases where this is not true. The most notable case applies when very different catalysts are compared, such as different pure metals. Although Norskov et al.[25] recently stressed why the d-band center would not correlate with the ORR activity for very different metals, this opinion is not widely spread within the scientific community. Indeed, a number of papers have been published and continue to be published ignoring this limitation of the d-band theory.

The second case of poor correlation between binding energy and d-band center applies when comparing the same metal but with different surface plane orientations. Many recently published works have not checked if the d-band center correlates well with the binding energy. Without this check, the validity of a quantitative relationship between the catalytic activity and d-band center is questionable.

Some nonpure metal catalysts, such as the Pt-sandwich catalyst,[9,41] are not limited by the correlated binding energy of O and OH observed in pure metal catalysts. As such, it is possible to have alloy catalysts with optimal O binding without changing the OH binding energy and vice versa. There is still a multitude of possible binary, ternary, and so on alloy configurations yet to be explored that can improve on the presently known ORR catalysts.

■ ASSOCIATED CONTENT

Supporting Information

Lattice parameters used for bulk and surface calculations, the most favorable binding sites for the pure metals, OH binding energy on the (100) surface for listed metals and the most favorable binding positions, calculated barriers of the ORR surface reactions for the Pt (100) surface, and a figure representing calculated O and OH binding energies of Pt-monolayer catalysts. This material is available free of charge via the Internet at http://pubs.acs.org.

■ AUTHOR INFORMATION

Corresponding Author

*E-mail: merinov@wag.caltech.edu (B.V.M.); wag@wag.caltech.edu (W.A.G.). Tel.: 1-626-3952754 (B.V.M.); 1-626-3952731 (W.A.G.).

Notes

The authors declare no competing financial interest.

■ ACKNOWLEDGMENTS

We gratefully acknowledge funding by the U.S. Department of Energy, Prime Contract No. DE-AC02-06CH11357 (ANL) and ANL Subcontract Nos. 7F-01041 (UNLV) and 7F-01321 (Caltech), and National Science Foundation (Grant CBET-1067848, Caltech). The facilities of the Materials and Process Simulation Center used in this study were established with grants from DURIP-ONR, DURIP-ARO, and NSF-CSEM.

■ REFERENCES

(1) Hüfner, S.; Wertheim, G. K. X-ray Photoemission Studies of 3D Metals from Mn to Cu. *Phys. Lett. A* **1974**, *47*, 349−350.
(2) Battye, F. L.; Goldmann, A.; Kasper, L.; Hüfner, S. Photoelectron-Spectra of Noble-Metals. *Z. Phys. B* **1977**, *27*, 209−217.
(3) Ruban, A.; Hammer, B.; Stoltze, P.; Skriver, H. L.; Norskov, J. K. Surface Electronic Structure and Reactivity of Transition and Noble Metals. *J. Mol. Catal. A: Chem.* **1997**, *115*, 421−429.
(4) Hammer, B.; Norskov, J. K. Electronic Factors Determining the Reactivity of Metal Surfaces. *Surf. Sci.* **1995**, *343*, 211−220.
(5) Markovic, N. M.; Ross, P. N. Surface Science Studies of Model Fuel Cell Electrocatalysts. *Surf. Sci. Rep.* **2002**, *45*, 121−229.
(6) Stamenkovic, V. R.; Mun, B. S.; Mayrhofer, K. J. J.; Ross, P. N.; Markovic, N. M. Effect of Surface Composition on Electronic Structure, Stability, and Electrocatalytic Properties of Pt-Transition Metal Alloys: Pt-Skin versus Pt-Skeleton Surfaces. *J. Am. Chem. Soc.* **2006**, *128*, 8813−8819.
(7) Stamenkovic, V. R.; Mun, B. S.; Arenz, M.; Mayrhofer, K. J. J.; Lucas, C. A.; Wang, G. F.; Ross, P. N.; Markovic, N. M. Trends in Electrocatalysis on Extended and Nanoscale Pt-Bimetallic Alloy Surfaces. *Nat. Mater.* **2007**, *6*, 241−247.
(8) Zhang, J.; Vukmirovic, M. B.; Ye, X.; Mavrikakis, M.; Adzic, R. R. Controlling the Catalytic Activity of Platinum-Monolayer Electrocatalysts for Oxygen Reduction with Different Substrates. *Angew. Chem., Int. Ed.* **2005**, *44*, 2132−2135.
(9) Menning, C. A.; Hwu, H. H.; Chen, J. G. G. Experimental and Theoretical Investigation of the Stability of Pt-3d-Pt(111) Bimetallic Surfaces under Oxygen Environment. *J. Phys. Chem. B* **2006**, *110*, 15471−15477.
(10) Mun, B. S.; Watanabe, M.; Rossi, M.; Stamenkovic, V.; Markovic, N. M.; Ross, P. N. A Study of Electronic Structures of Pt_3M (M = Ti, V, Cr, Fe, Co, Ni) Polycrystalline Alloys with Valence-Band Photoemission Spectroscopy. *J. Chem. Phys.* **2005**, *123*, 204717−204720.
(11) Norskov, J. K.; Stamenkovic, V.; Mun, B. S.; Mayrhofer, K. J. J.; Ross, P. N.; Markovic, N. M.; Rossmeisl, J.; Greeley, J. Changing the Activity of Electrocatalysts for Oxygen Reduction by Tuning the Surface Electronic Structure. *Angew. Chem., Int. Ed.* **2006**, *45*, 2897−2901.
(12) Stamenkovic, V.; Schmidt, T. J.; Ross, P. N.; Markovic, N. M. Surface Composition Effects in Electrocatalysis: Kinetics of Oxygen Reduction on Well-Defined Pt_3Ni and Pt_3Co Alloy Surfaces. *J. Phys. Chem. B* **2002**, *106*, 11970−11979.
(13) Gauthier, Y. Pt-Metal Alloy Surfaces: Systematic Trends. *Surf. Rev. Lett.* **1996**, *3*, 1663−1689.

(14) Stamenkovic, V. R.; Fowler, B.; Mun, B. S.; Wang, G. F.; Ross, P. N.; Lucas, C. A.; Markovic, N. M. Improved Oxygen Reduction Activity on $Pt_3Ni(111)$ via Increased Surface Site Availability. *Science* **2007**, *315*, 493−497.
(15) Greeley, J.; Stephens, I. E. L.; Bondarenko, A. S.; Johansson, T. P.; Hansen, H. A.; Jaramillo, T. F.; Rossmeisl, J.; Chorkendorff, I.; Norskov, J. K. Alloys of Platinum and Early Transition Metals as Oxygen Reduction Electrocatalysts. *Nat. Chem.* **2009**, *1*, 552−556.
(16) Yu, T. H.; Sha, Y.; Merinov, B. V.; Goddard, W. A. Improved Non-Pt Alloys for the Oxygen Reduction Reaction at Fuel Cell Cathodes Predicted from Quantum Mechanics. *J. Phys. Chem. C* **2010**, *114*, 11527−11533.
(17) Wang, X. P.; Kariuki, N.; Vaughey, J. T.; Goodpaster, J.; Kumar, R.; Myers, D. J. Bimetallic Pd-Cu Oxygen Reduction Electrocatalysts. *J. Electrochem. Soc.* **2008**, *155*, B602−B609.
(18) Sarkar, A.; Murugan, A. V.; Manthiram, A. Low Cost Pd-W Nanoalloy Electrocatalysts for Oxygen Reduction Reaction in Fuel Cells. *J. Mater. Chem.* **2009**, *19*, 159−165.
(19) Vukmirovic, M. B.; Zhang, J.; Sasaki, K.; Nilekar, A. U.; Uribe, F.; Mavrikakis, M.; Adzic, R. R. Platinum Monolayer Electrocatalysts for Oxygen Reduction. *Electrochim. Acta* **2007**, *52*, 2257−2263.
(20) Lima, F. H. B.; Zhang, J.; Shao, M. H.; Sasaki, K.; Vukmirovic, M. B.; Ticianelli, E. A.; Adzic, R. R. Catalytic Activity - d-Band Center Correlation for the O_2 Reduction Reaction on Platinum in Alkaline Solutions. *J. Phys. Chem. C* **2007**, *111*, 404−410.
(21) Kitchin, J. R.; Norskov, J. K.; Barteau, M. A.; Chen, J. G. Modification of the Surface Electronic and Chemical Properties of Pt(111) by Subsurface 3d Transition Metals. *J. Chem. Phys.* **2004**, *120*, 10240−10246.
(22) Nilsson, A.; Pettersson, L. G. M.; Hammer, B.; Bligaard, T.; Christensen, C. H.; Norskov, J. K. The Electronic Structure Effect in Heterogeneous Catalysis. *Catal. Lett.* **2005**, *100*, 111−114.
(23) Tamura, M.; Kon, K.; Satsuma, A.; Shimizu, K. Volcano-Curves for Dehydrogenation of 2-Propanol and Hydrogenation of Nitrobenzene by SiO_2-Supported Metal Nanoparticles Catalysts as Described in Terms of a d-Band Model. *ACS Catal.* **2012**, *2*, 1904−1909.
(24) Hofmann, T.; Yu, T. H.; Folse, M.; Weinhardt, L.; Bar, M.; Zhang, Y. F.; Merinov, B. V.; Myers, D. J.; Goddard, W. A.; Heske, C. Using Photoelectron Spectroscopy and Quantum Mechanics to Determine d-Band Energies of Metals for Catalytic Applications. *J. Phys. Chem. C* **2012**, *116*, 24016−24026.
(25) Abild-Pedersen, F.; Nilsson, A.; Norskov, J. K. Comment on "Using Photoelectron Spectroscopy and Quantum Mechanics to Determine d-Band Energies of Metals for Catalytic Applications". *J. Phys. Chem. C* **2013**, *117*, 6914−6915.
(26) Jia, Q. Y.; Segre, C. U.; Ramaker, D.; Caldwell, K.; Trahan, M.; Mukerjee, S. Structure-Property-Activity Correlations of Pt-Bimetallic Nanoparticles: A Theoretical Study. *Electrochim. Acta* **2013**, *88*, 604−613.
(27) Hofmann, T.; Yu, T. H.; Folse, M.; Weinhardt, L.; Bar, M.; Zhang, Y.; Merinov, B. V.; Myers, D. J.; Goddard, W. A.; Heske, C. Using Photoelectron Spectroscopy and Quantum Mechanics to Determine d-Band Energies of Metals for Catalytic Applications. *J. Phys. Chem. C* **2012**, *116*, 24016.
(28) Sha, Y.; Yu, T. H.; Merinov, B.; Shirvanian, P.; Goddard, W. A. Oxygen Hydration Mechanism for the Oxygen Reduction Reaction at Pt and Pd Fuel Cell Catalysts. *J. Phys. Chem. Lett.* **2011**, *2*, 572−576.
(29) Jacob, T.; Goddard, W. A. Water Formation on Pt and Pt-Based Alloys: A Theoretical Description of a Catalytic Reaction. *ChemPhysChem* **2006**, *7*, 992−1005.
(30) Norskov, J. K.; Rossmeisl, J.; Logadottir, A.; Lindqvist, L.; Kitchin, J. R.; Bligaard, T.; Jonsson, H. Origin of the Overpotential for Oxygen Reduction at a Fuel-Cell Cathode. *J. Phys. Chem. B* **2004**, *108*, 17886−17892.
(31) Janik, M. J.; Taylor, C. D.; Neurock, M. First-Principles Analysis of the Initial Electroreduction Steps of Oxygen over Pt(111). *J. Electrochem. Soc.* **2009**, *156*, B126−B135.
(32) Sha, Y.; Yu, T. H.; Merinov, B.; Shirvanian, P.; Goddard, D. Mechanism for Oxygen Reduction Reaction on Pt_3Ni Alloy Fuel Cell Cathode. *J. Phys. Chem. C* **2012**, *116*, 21334−21342.
(33) Schultz, P. *SEQQUEST, Electronic Structure Code*; Sandia National Laboratory: Albuquerque, NM, http://dft.sandia.gov/Quest/.
(34) Edwards, A. *SEQQUEST, Post Analysis Code*; Sandia National Laboratory: Albuquerque, NM, http://dft.sandia.gov/Quest/.
(35) Perdew, J. P.; Burke, K.; Ernzerhof, M. Generalized Gradient Approximation Made Simple. *Phys. Rev. Lett.* **1996**, *77*, 3865−3868.
(36) Perdew, J. P.; Zunger, A. Self-Interaction Correction to Density-Functional Approximations for Many-Electron Systems. *Phys. Rev. B* **1981**, *23*, 5048−5079.
(37) Melius, C. F.; Goddard, W. A. Ab Initio Effective Potentials for Use in Molecular Quantum-Mechanics. *Phys. Rev. A* **1974**, *10*, 1528−1540.
(38) Goddard, W. A. New Foundation for Use of Pseudopotentials in Metals. *Phys. Rev.* **1968**, *174*, 659−662.
(39) Mills, G.; Jonsson, H. Quantum and Thermal Effects in H-2 Dissociative Adsorption: Evaluation of Free-Energy Barriers in Multidimensional Quantum-Systems. *Phys. Rev. Lett.* **1994**, *72*, 1124−1127.
(40) See Supporting Information at http://pubs.acs.org for lattice parameters, binding geometries, Pt (100) barriers, and additional Pt monolayer binding energies.
(41) Xin, H.; Linic, S. Exceptions to the d-Band Model of Chemisorption on Metal Surfaces: The Dominant Role of Repulsion between Adsorbate States and Metal d-States. *J. Chem. Phys.* **2010**, *132*, 221101−221104.
(42) Ford, D. C.; Nilekar, A. U.; Xu, Y.; Mavrikakis, M. Partial and Complete Reduction of O_2 by Hydrogen on Transition Metal Surfaces. *Surf. Sci.* **2010**, *604*, 1565−1575.
(43) Gajdos, M.; Eichler, A.; Hafner, J. CO Adsorption on Close-Packed Transition and Noble Metal Surfaces: Trends from Ab Initio Calculations. *J. Phys.: Condens. Matter* **2004**, *16*, 1141−1164.
(44) Haydock, R.; Kelly, M. J. Surface Densities of States in Tight-Binding Approximations. *Surf. Sci.* **1973**, *38*, 139−148.
(45) Hwang, S. J.; Yoo, S. J.; Jang, S.; Lim, T. H.; Hong, S. A.; Kim, S. K. Ternary Pt-Fe-Co Alloy Electrocatalysts Prepared by Electrodeposition: Elucidating the Roles of Fe and Co in the Oxygen Reduction Reaction. *J. Phys. Chem. C* **2011**, *115*, 2483−2488.